Published online 20 November 2018

Nucleic Acids Research, 2019, Vol. 47, No. 1 ***237–252***
doi: 10.1093/nar/gky1154

A genetic screen pinpoints ribonucleotide reductase residues that sustain dNTP homeostasis and specifies a highly mutagenic type of dNTP imbalance

Tobias T. Schmidt[1,2], Sushma Sharma[3], Gloria X. Reyes[1], Kerstin Gries[1], Maike Gross[1], Boyu Zhao[1,2], Jui-Hung Yuan[4], Rebecca Wade[4,5,6], Andrei Chabes[3,7] and Hans Hombauer[1,*]

[1]DNA Repair Mechanisms and Cancer, German Cancer Research Center (DKFZ), Heidelberg D-69120, Germany, [2]Faculty of Bioscience, Heidelberg University, Heidelberg D-69120, Germany, [3]Department of Medical Biochemistry and Biophysics, Umeå University, Umeå SE-901 87 Sweden, [4]Molecular and Cellular Modeling Group, Heidelberg Institute for Theoretical Studies (HITS), Heidelberg D-69118, Germany, [5]Interdisciplinary Center for Scientific Computing (IWR), Heidelberg D-69120, Germany, [6]Center for Molecular Biology of the University of Heidelberg (ZMBH), DKFZ-ZMBH Alliance, Heidelberg D-69120, Germany and [7]Laboratory for Molecular Infection Medicine Sweden, Umeå University, Umeå SE-901 87, Sweden

Received September 06, 2018; Revised October 25, 2018; Editorial Decision October 26, 2018; Accepted October 29, 2018

ABSTRACT

The balance and the overall concentration of intracellular deoxyribonucleoside triphosphates (dNTPs) are important determinants of faithful DNA replication. Despite the established fact that changes in dNTP pools negatively influence DNA replication fidelity, it is not clear why certain dNTP pool alterations are more mutagenic than others. As intracellular dNTP pools are mainly controlled by ribonucleotide reductase (RNR), and given the limited number of eukaryotic *RNR* mutations characterized so far, we screened for *RNR1* mutations causing mutator phenotypes in *Saccharomyces cerevisiae*. We identified 24 *rnr1* mutant alleles resulting in diverse mutator phenotypes linked in most cases to imbalanced dNTPs. Among the identified *rnr1* alleles the strongest mutators presented a dNTP imbalance in which three out of the four dNTPs were elevated (dCTP, dTTP and dGTP), particularly if dGTP levels were highly increased. These *rnr1* alleles caused growth defects/lethality in DNA replication fidelity-compromised backgrounds, and caused strong mutator phenotypes even in the presence of functional DNA polymerases and mismatch repair. In summary, this study pinpoints key residues that contribute to allosteric regulation of RNR's overall activity or substrate specificity. We propose a model that distinguishes between different dNTP pool alterations and provides a mechanistic explanation why certain dNTP imbalances are particularly detrimental.

INTRODUCTION

DNA replication errors are prevented by DNA polymerases that select and incorporate the correct dNTP, but also proofread base pairing according to the Watson-Crick model. To further increase the fidelity of this process, most organisms possess a DNA mismatch repair (MMR) system that recognizes and excises incorrectly incorporated nucleotides (1–3). Another important determinant of DNA replication fidelity is the proper balance and overall concentration of dNTPs, both primarily regulated by ribonucleotide reductase (RNR) (4–6). Eukaryotic RNR is a multimeric enzyme (with the minimal unit composed of two large α subunits and two smaller β subunits) that catalyzes the reduction of ribonucleoside diphosphates (rNDPs) into the corresponding deoxyribonucleoside diphosphates (dNDPs) (6–8). In most eukaryotes, RNR activity is controlled at multiple levels including: transcriptional, spatial (regulating the cellular compartmentalization of different RNR subunits) and through allosteric regulation. The overall enzymatic activity and the substrate specificity are controlled by their respective allosteric sites (6,9,10). The site that regulates the overall activity is called the 'activity site' (A-site) and it serves as an on/off switch in response to the binding of the effectors ATP or dATP (ATP works as an activator and dATP as an inhibitor) (7). The second allosteric site, referred to as the 'substrate specificity site' (S-site), determines which substrate (rNDP) is going to be reduced at the 'catalytic site' (C-site). Substrate specificity is accom-

*To whom correspondence should be addressed. Tel: +49 6221 42 3239; Fax: +49 6221 42 3237; Email: h.hombauer@dkfz.de

plished by partially characterized protein conformational changes triggered upon binding of nucleotide effectors at the S-site. These conformational changes prime the C-site for specific substrates. Thus, ATP or dATP binding at the S-site favors CDP and UDP reduction, whereas dTTP and dGTP promote GDP and ADP reduction, respectively (7). Previously, the yeast Rnr1 crystal structure was used to predict mutations that may interfere with RNR's allosteric regulation by altering a flexible loop (loop 2) that interconnects the S-site with the C-site (11). Characterization of yeast strains expressing these *rnr1* mutations revealed severe dNTP imbalances, some of them associated with extreme growth defects and S-phase checkpoint activation. Although all characterized mutations resulted in increased mutation rates, the small number of examples could not explain why certain dNTP pool alterations were more detrimental for DNA replication fidelity than others (11,12).

To gain a more comprehensive understanding of how different *rnr1* mutations affect dNTP homeostasis and DNA replication fidelity *in vivo*, we randomly mutagenized yeast *RNR1* gene to search for mutations causing increased mutagenesis. A similar approach has been successfully used in the past for the identification of mutations in *Escherichia coli* (*E. coli*) ribonucleotide reductase genes *NrdA* and *NrdB* (13). To increase the chances of identifying *rnr1* mutations causing strong as well as weak mutator phenotypes, we screened for *rnr1* mutations in an exonuclease 1 deficient (*exo1Δ*) background. Exo1 is a 5′ to 3′ double stranded DNA exonuclease that participates in different DNA repair transactions including recombination, double strand break repair, MMR and post-replication repair (PRR) (14,15). *exo1Δ* mutants show a mild mutator phenotype that can be exacerbated by mutations compromising DNA replication fidelity or repair (16–18). A previous random mutagenesis screen performed in an *exo1Δ* strain (16) identified a number of *exo1Δ*-dependent mutator mutants, including among others, several hypomorphic MMR mutants, and one Rnr1 mutant (*rnr1-G271S*) that was not characterized at that point to a large extent. Therefore, we hypothesized that screening for *rnr1* mutations in an *exo1Δ* background may uncover novel *rnr1* alleles that compromise DNA replication fidelity. In agreement with our expectations, we identified a collection of *rnr1* mutations that strongly exacerbated *exo1Δ* mutator phenotype. Most mutations were located at or near the S-site, affecting residues predicted to be in direct contact with the dNTP effector. Other mutations were located at the A-site, near the C-site or at two α-helices at the Rnr1-Rnr1 dimer interphase. Quantitative analysis of dNTP concentrations in yeast strains expressing *rnr1* mutant alleles showed either dNTP imbalances or an overall increase in dNTP levels. Mutation rate analysis, as well as genetic interaction studies revealed that dNTP pool imbalances having elevated three out of the four dNTPs are particularly detrimental for DNA replication fidelity and survival. Among the *rnr1* mutations causing a '*3 out of 4*' imbalance we found that the most mutagenic ones were those with the highest dGTP concentrations. This type of imbalance causes mispairs and frameshift deletion mutations that frequently escape DNA polymerase proofreading and MMR. In summary, this study first, pinpoints to key residues that play important roles in the regulation of RNR's substrate specificity and activity, and secondly, it specifies which dNTP alterations are more detrimental for DNA replication fidelity.

MATERIALS AND METHODS

All *S. cerevisiae* strains used in this study (Supplementary Table S7) are derivatives of the S288C strain RDKY3686 (*MATα ura3-52 leu2Δ1 trp1Δ63 hom3-10 his3Δ200 lys2-10A*) (16) or RDKY5964 (a *MAT*a version of RDKY3686) (19). Strains were cultivated at 30°C according to standard protocols. Gene deletions and gene tagging were performed using standard PCR-based recombination methods (20,21), followed by confirmation by PCR. Specific *rnr1* mutations were introduced at the *RNR1* chromosomal locus by pop-in/pop-out strategy and the presence of the desired mutations, as well as the absence of additional unwanted mutations was confirmed by sequencing (for details, see Supplementary Data).

Random *rnr1* mutagenesis screen

The *RNR1* gene was randomly mutagenized by PCR, using a similar strategy as previously described (22). Briefly, *RNR1* (including some vector related sequences) was amplified by PCR under mutagenic conditions and co-transformed together with a linearized plasmid (*CEN6, ARSH4, LEU2*) into HHY6555 (*MAT*a *ura3-52 leu2Δ1 trp1Δ63 hom3-10 his3Δ200 lys2-10A rnr1::kanMX4 exo1::hphNT1 lig4::HIS3* + pHHB560) for *in vivo* gap repair. Leu^+ transformants were grown on 5-FOA to eliminate the WT-*RNR1* plasmid by plasmid shuffling (23), and then screened *in vivo* for mutator phenotypes with frameshift reporters (*lys2-10A* and *hom3-10*) and one general mutator reporter (*CAN1* inactivation) (16,24). Plasmids resulting in increased mutagenesis were identified, sequenced for *rnr1* mutations (Supplementary Table S8) and retransformed in HHY6214 and HHY6551 for further analysis. For details about strain construction and screening strategy, see Supplementary Data).

Determination of mutation rates

Mutation rates using frameshift reversion (*hom3-10* and *lys2-10A*) and *CAN1* inactivation assay were determined by fluctuation analysis as described previously (16,24). Mutation rates were determined based on two biological isolates and at least 14 independent cultures.

Determination of rNTP and dNTP pools

rNTP and dNTPs were measured as described in (17,25).

Synthetic growth defect/lethality analysis by plasmid shuffling

Genetic interactions resulting in growth defects (GD) or synthetic lethal (SL) interactions between *rnr1*- and DNA replication fidelity/checkpoint-mutant alleles were identified by plasmid shuffling experiments. We generated yeast strains lacking chromosomal *RNR1* gene (complemented

by a WT-*RNR1-URA3* plasmid) and indicated additional gene deletions/mutations. These strains were transformed with plasmids (*ARSH4-CEN6, LEU2*) expressing the WT-*RNR1* or mutant *rnr1* alleles. Overnight cultures were spotted in serial dilutions on medium lacking leucine and containing 5-FOA. Plates were incubated for 4 days at 30°C, imaged (GelDoc System, Bio-Rad) and scored visually.

Yeast cell lysates and immunoblotting

Saccharomyces cerevisiae whole-cell protein extracts were generated as previously described (19) and analyzed on 4–15% Mini-PROTEAN TGX precast gels (Bio-Rad) followed by immunoblotting using anti-Rnr1 (AS09576, Agrisera), anti-Rnr2 (AS09575, Agrisera) anti-Rnr3 (AS09574, Agrisera) and anti-tubulin/anti-Rnr4 (YL1/2, Sigma).

DNA content analysis

Logarithmic *S. cerevisiae* cultures were processed as described in (26) and analyzed using BD FACS Canto II (BD Biosciences). Percentage of cells in S phase was determined using FlowJo (v10.1, Tree Star Inc.) cell cycle analysis plug-in.

Live-cell imaging of Pms1-GFP foci

Exponentially growing cells were processed and imaged as described in (19) using a DeltaVision Elite imaging system (Applied Precision). Three independent biological replicates were analyzed per genotype and Mann-Whitman test was used to compare different genotypes.

CAN1 and *URA3* mutation spectra analysis

The *CAN1* or the *URA3* gene of independent Can^R or 5-FOA^R colonies, respectively, was amplified from genomic DNA by PCR and sequenced (GATC). Sequences were analyzed with Lasergene 12 (DNASTAR). Mutation spectra and mutational hotspots were compared by Fisher's exact test in R. Values of $P \leq 0.05$ were defined as significantly different.

RESULTS

An *RNR1* mutagenesis screen identifies mutations causing Exo1-dependent and Exo1-independent mutator phenotypes

We performed a gene-specific screen for *rnr1* mutations that exacerbate *exo1Δ* mutator phenotype (Supplementary Figure S1A). First, we generated a plasmid library of randomly mutagenized yeast *RNR1 (rnr1, ARS-CEN, LEU2)* by using mutagenic-PCR and *in vivo* gap-repair (22). This *RNR1* mutant library was then used to replace a wild-type (WT) *RNR1-URA3* plasmid in an *rnr1Δ exo1Δ* strain by plasmid shuffling (23). For the identification of *rnr1* mutant plasmids resulting in mutator phenotypes, we took advantage of three *in vivo* mutational reporters: the forward inactivation assay *CAN1* and two frameshift reversion reporters (*lys2-10A* and *hom3-10*). The *CAN1* inactivation assay serves as a general mutator assay, as *CAN1* inactivation can result from base substitutions, frameshifts or even gross chromosomal rearrangements, giving rise to canavanine resistant colonies (Can^R). In contrast, the *lys2-10A* and *hom3-10* frameshift reversion assays are extremely sensitive to single nucleotide deletion events due to DNA polymerase slippage (–1 nucleotide deletions) that occur in a well-defined mononucleotide run, resulting in lysine (Lys^+) and threonine (Thr^+) prototrophic colonies, respectively. As result of three independent screens, and having tested for mutator phenotype approximately 39,000 Leu^+ transformants, we identified 272 *rnr1* mutant plasmids that conferred a mutator phenotype when they were retransformed in the *rnr1Δ exo1Δ* strain. DNA sequencing of *RNR1* gene of the 272 confirmed mutator plasmids revealed a variety of mutations resulting in single and multiple amino acid substitutions. For those plasmids containing two missense mutations, we identified 'passenger' mutations (that did not contribute to the mutator phenotype) by creating plasmids containing each of both point mutations by site directed mutagenesis or subcloning. These plasmids were compared side-by-side for mutator phenotype with the corresponding plasmids containing multiple mutations initially isolated in our screen. After excluding plasmids containing redundant mutants and those resulting in more than two amino acid substitutions, we obtained 24 unique *rnr1* mutant alleles causing increased mutagenesis (Table 1). Out of the 24 identified *rnr1* alleles (Table 1), 16 of them harbor a single point mutation resulting in one amino acid substitution responsible of the mutator phenotype. The remaining plasmids contain mutations resulting in two amino acid substitutions, both of which were required to induce increased mutagenesis. In agreement with the high sequence conservation between *S. cerevisiae* and human RNR (about 67% protein identity), 21 out of 22 affected residues are conserved between both species (Figure 1A) and remarkably, four of them (A245, R256, A283 and Y285) have been found mutated in human tumor samples (cBioportal for Cancer Genomics and/or the Catalog of somatic mutations in cancer databases).

Eleven out of the 24 *rnr1* alleles were recovered independently more than once. For example, *rnr1-S269P, rnr1-Y285C, rnr1-K243E* and *rnr1-T265A* mutations were identified 14-, 10-, 10- and 9-times in independent yeast transformants. These observations are in agreement with a high degree of saturation of the mutagenesis screen, suggesting that under our experimental conditions it is unlikely that many *rnr1* mutations remain unidentified. Interestingly, almost all mutations clustered within amino acids 226 and 291 (Figure 1A), a region that comprises two flexible loops (loop 1 and 2) with important functions in RNR allosteric regulation (6,27,28). About half of the residues affected by mutations (11 out 23) located at or near the S-site (Figure 1B) where they engage in hydrogen-bonding and other electrostatic interactions with several atoms of the bound effector (Figure 1C and D). We also identified two mutations (*rnr1-G8D* and *rnr1-F15S*) affecting residues located at the A-site (Figure 1B and E), and two others more closely located at the C-site (*rnr1- A245V* and *rnr1-S425L*). Moreover, some mutations (e.g. *rnr1-S242T, rnr1-M275T* and *rnr1-T282A*) affected residues located in one of two α-helices at the Rnr1-Rnr1 dimer interface. First, we validated the identified mutator phenotypes by measuring mutation rates in

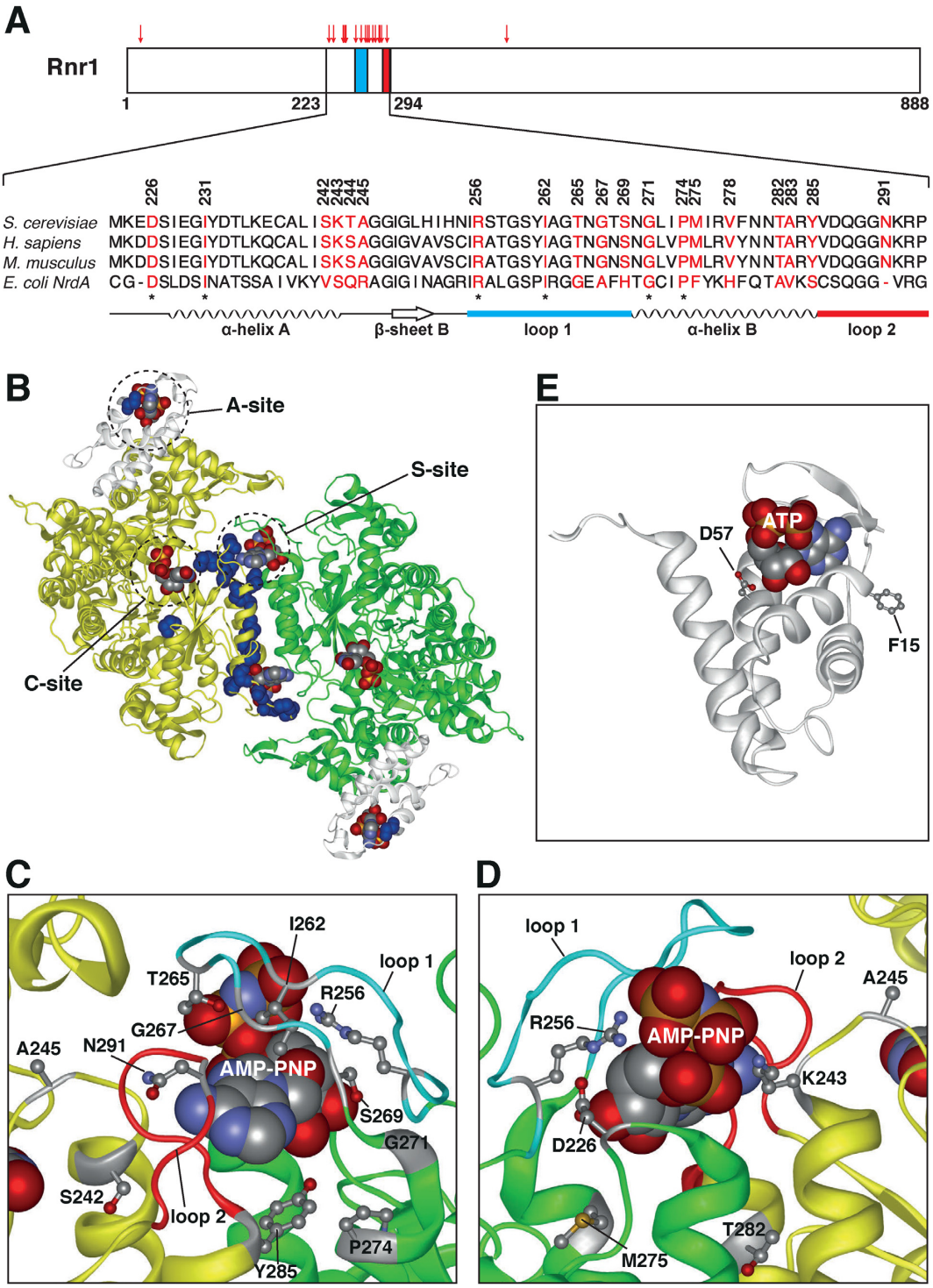

Figure 1. *rnr1* mutations that cause increased mutator phenotypes in an *exo1Δ* mutant cluster in the Rnr1 S-site. (**A**) Schematic representation of Rnr1 protein indicating the position of amino acids affected by *rnr1* mutations (red arrows). Loop 1 and loop 2 are shown in cyan and red boxes, respectively. Below, sequence alignment of Rnr1 from *S. cerevisiae* (amino acids 223–294) with *H. sapiens*, *M. musculus* and *E. coli NrdA* homologs. Amino acids affected by mutations are marked in red. Asterix (*) denotes conservation across all four species. (**B**) Structural model of *S. cerevisiae* Rnr1 dimer (PDB: 2CVV) (28) indicating the position of amino acids affected by mutations identified in this study as blue spheres, in one of the two RNR monomers (shown in yellow and green). In addition, in this model the A-site of human RNR (hRRM1), shown in grey, has been superimposed (PDB: 3HNE, residues 1–94, in complex with ATP). (**C**) Front and (**D**) back views of the S-site structure from *S. cerevisiae* (PDB: 2CVV). Mutations identified in this screen are indicated as ball and sticks. Loop 1 and 2 are shown in cyan and red, respectively. (**E**) Ribbon diagram depicting the human RNR A-site composed by a four-helix bundle forming an ATP-binding cone covered by a β-hairpin (PDB: 3HNE, residues 1–94, ATP bound) (39). Residues Phe15 (F15) and Asp57 (D57) are represented as ball and sticks. See text for more details. Figures B-E were made using indicated Protein Data Bank (PDB) entries, rendered with *Protean 3D*, Lasergene 15.1 DNASTAR.

Table 1. Mutation rates caused by *rnr1* mutations expressed on a centromeric plasmid in the *exo1Δ rnr1Δ* double mutant strain

	Mutation Rate (fold increase)*		
Allele†	Can^R	Thr^+	Lys^+
+ *RNR1-WT*	1.7 [1.5–3.0] × 10^{-6} (1)	2.4 [1.8–3.2] × 10^{-8} (1)	2.2 [1.6–3.0] × 10^{-7} (1)
+ *rnr1-G8D,V278A*	3.5 [3.1–4.9] × 10^{-6} (2)	2.5 [1.6–3.5] × 10^{-7} (10)	4.0 [2.8–8.6] × 10^{-6} (19)
+ *rnr1-F15S*	2.6 [1.9–3.9] × 10^{-5} (16)	3.8 [2.7–5.0] × 10^{-6} (158)	3.2 [2.6–5.8] × 10^{-6} (15)
+ *rnr1-D226G*	1.3 [0.4–1.8] × 10^{-4} (80)	1.8 [0.9–3.5] × 10^{-4} (7523)	9.3 [5.3–25.9] × 10^{-5} (424)
+ *rnr1-D226V*	1.1 [0.6–1.7] × 10^{-4} (66)	1.9 [0.7–3.2] × 10^{-4} (7737)	1.6 [0.7–2.8] × 10^{-4} (753)
+ *rnr1- D226N,S117P*‡	4.5 [3.0–9.0] × 10^{-5} (27)	1.1 [0.4–2.8] × 10^{-4} (4612)	1.4 [1.0–1.9] × 10^{-4} (645)
+ *rnr1-I231T,T244A*	8.4 [6.9–11.0] × 10^{-6} (5)	3.3 [2.3–5.2] × 10^{-6} (137)	3.3 [2.9–4.5] × 10^{-5} (150)
+ *rnr1-S242T*	4.5 [3.1–7.7] × 10^{-5} (27)	9.5 [6.4–16.3] × 10^{-6} (396)	1.6 [1.3–2.8] × 10^{-4} (750)
+ *rnr1-K243E*	1.0 [0.8–1.2] × 10^{-4} (63)	3.9 [2.6–8.1] × 10^{-5} (1613)	2.6 [1.8–4.9] × 10^{-4} (1185)
+ *rnr1-T244I,V278A*	1.4 [0.9–2.5] × 10^{-5} (8)	1.0 [0.8–2.1] × 10^{-5} (423)	5.7 [1.3–11.0] × 10^{-5} (262)
+ *rnr1-A245V*	1.3 [0.9–2.3] × 10^{-5} (8)	5.0 [2.8–11.7] × 10^{-6} (207)	3.4 [2.1–6.6] × 10^{-6} (16)
+ *rnr1-R256H, Y779C*	2.3 [1.3–3.6] × 10^{-5} (14)	2.9 [1.9–5.6] × 10^{-5} (1214)	1.6 [0.9–2.4] × 10^{-4} (741)
+ *rnr1-I262T,M275I*	1.1 [0.8–1.9] × 10^{-4} (69)	2.0 [0.7–2.6] × 10^{-4} (8165)	4.5 [3.0–11.2] × 10^{-4} (2077)
+ *rnr1-I262V,N291D*	6.4 [4.5–9.6] × 10^{-5} (39)	1.7 [1.0–2.8] × 10^{-5} (711)	1.8 [1.2–2.8] × 10^{-4} (815)
+ *rnr1-I262V*	2.8 [2.1–3.4] × 10^{-6} (2)	2.8 [2.2–3.1] × 10^{-7} (12)	3.3 [1.8–6.3] × 10^{-6} (15)
+ *rnr1-T265A*	6.3 [3.9–7.9] × 10^{-6} (4)	1.9 [0.9–4.1] × 10^{-6} (81)	3.3 [1.1–5.9] × 10^{-5} (153)
+ *rnr1-G267C*	3.9 [2.2–7.8] × 10^{-5} (23)	1.0 [0.6–2.0] × 10^{-5} (428)	2.1 [1.8–2.8] × 10^{-4} (957)
+ *rnr1-S269P*	8.4 [6.6–13.0] × 10^{-5} (51)	2.1 [1.2–4.1] × 10^{-4} (8595)	2.8 [2.0–4.3] × 10^{-4} (1276)
+ *rnr1-G271S*	3.7 [3.4–4.5] × 10^{-6} (2)	1.1 [0.9–1.2] × 10^{-6} (47)	1.7 [1.4–3.6] × 10^{-6} (8)
+ *rnr1-P274L*	5.9 [3.9–10.2] × 10^{-6} (4)	9.4 [5.5–11.5] × 10^{-7} (39)	2.7 [1.7–3.9] × 10^{-5} (123)
+ *rnr1-M275T*	1.8 [1.0–2.4] × 10^{-6} (1)	2.6 [2.0–4.3] × 10^{-7} (11)	2.1 [1.3–6.3] × 10^{-6} (9)
+ *rnr1-T282A*	2.9 [2.4–4.6] × 10^{-6} (2)	1.0 [0.8–1.5] × 10^{-7} (4)	2.0 [1.6–2.2] × 10^{-6} (9)
+ *rnr1-T282S*	3.3 [2.4–6.4] × 10^{-6} (2)	3.3 [2.3–6.4] × 10^{-7} (14)	3.0 [1.5–5.5] × 10^{-5} (138)
+ *rnr1-A283V,S425L*	8.2 [6.4–9.4] × 10^{-6} (5)	1.1 [0.9–1.5] × 10^{-6} (48)	3.1 [2.1–6.4] × 10^{-5} (140)
+ *rnr1-Y285C*	1.1 [0.8–1.3] × 10^{-5} (7)	4.5 [3.5–7.1] × 10^{-6} (187)	7.7 [6.4–13.0] × 10^{-5} (35)
msh2Δ + *RNR1-WT*	4.0 [2.4–6.2] × 10^{-5} (24)	4.3 [2.4–7.9] × 10^{-5} (1789)	2.3 [1.5–2.7] × 10^{-4} (1032)

*Median rates for the *CAN1* (Can^R) inactivation assay and for *hom3-10* (Thr^+) and *lys2-10A* (Lys^+) frameshift reversion assays with 95% confidence interval in square brackets and fold increase in parentheses, relative to *rnr1Δ exo1Δ* strain complemented with the WT-*RNR1* plasmid.
†Allele expressed on a low-copy number plasmid in an *rnr1Δ exo1Δ* strain. As reference for total MMR deficiency an *rnr1Δ msh2Δ* strain complemented with the WT-*RNR1* plasmid was included. Site directed mutagenesis (or subcloning) was used to independently generate *rnr1* single point mutants for plasmids containing more than one mutation. ‡Indicates an expected passenger mutation that was not further validated.

the *rnr1Δ exo1Δ* strain complemented by mutant *rnr1* plasmids. Some mutations resulted in weak mutator phenotypes (e.g. *rnr1-A245V, rnr1-I262V, rnr1-M275T* or *rnr1-T282A*) causing a less than 10-fold increase in the *CAN1* inactivation assay, whereas others showed strong mutator phenotypes with increases up to 80-fold in *CAN1* inactivation (e.g. *rnr1-D226G, rnr1-K243E* and *rnr1-S269P*) (Table 1). Further complementation analysis in a *rnr1Δ EXO*1-WT background revealed that most *rnr1* alleles do not cause mutagenesis unless the *EXO1* gene was inactivated (Supplementary Figure S1B). Thus, under normal conditions cells largely compensate for the presumed dNTP alterations associated with these *rnr1* mutant alleles. Outstandingly, three *rnr1* mutant alleles (*rnr1-K243E, rnr1-I262V,N291D* and *rnr1-I262T,M275I*) (Supplementary Figure S1B) caused a strong frameshift mutator phenotype even in an Exo1-WT strain, indicating that these mutations can saturate or inactivate cellular mechanisms that deal with mutation avoidance.

Genetic interactions resulting in synthetic growth defect/lethality revealed *rnr1* mutants that depend on DNA polymerase proofreading and/or MMR function for survival

In yeast, extreme mutator phenotypes can lead to growth defects (GD) or synthetic lethality (SL) as soon as the mutation frequency exceeds an 'error extinction threshold' causing the inactivation of one essential gene per genome duplication (29,30). As some *rnr1* mutations in an *exo1Δ* mutant caused mutation rates that approximate the error-extinction threshold in haploid cells (10^{-3} mutations per cell division) (Table 1) (30), we asked whether *rnr1* mutant alleles may result in GD/SL in other DNA replication fidelity-compromised backgrounds. To evaluate this possibility, we introduced plasmids expressing *rnr1* mutations (by plasmid shuffling) (Supplementary Figure S2) in proofreading-defective DNA polymerase mutants (*pol2-04* and *pol3-01*) (29,31) and a MMR-deficient (*msh2Δ*) strain (24,32). As specific *rnr1* mutations can cause synthetic lethality in the absence of the DNA damage-inducible large RNR subunit Rnr3 (11), we also transformed this collection of *rnr1* mutant plasmids in an *rnr3Δ* strain, as well as in a strain lacking the DNA damage checkpoint kinase Dun1 (*dun1Δ*) (33) which activates Rnr3 expression. Out of the 24 *rnr1* alleles 17 of them resulted in one or more genetic interaction(s) resulting in GD/SL (summarized in Table 2, see also Supplementary Figure S2B). These genetic interactions were used to categorize the *rnr1* alleles into four different groups: Group 1. Mutations (*rnr1-G8D,V278A, rnr1-F15S, rnr1-I231T,T244A, rnr1-T244I,V278A, rnr1-I262V, rnr1-T265A*, *rnr1-P274L, rnr1-M275T*, *rnr1-T282A/S* and *rnr1-A283V,S425L*) that do not interact with any of the tested alleles or interact exclusively with *pol3-01*. In gen-

eral, these mutations caused weak mutator phenotypes in the *exo1Δ* background, most of them resulting in less than 10-fold increase in the *CAN1* inactivation rate (Table 1) and did not cause a frameshift mutator phenotype in the presence of Exo1 (Supplementary Figure S1). Group 2. Mutations (*rnr1-A245V, rnr1-G271S* and *rnr1-Y285C*) that exclusively interact with proofreading-defective DNA polymerases *pol3-01* and *pol2-04*. Similar to the previous group, these mutant alleles when expressed in the *exo1Δ* background resulted in a modest increase in the *CAN1* mutation rate, and no frameshift mutator phenotype in the presence of Exo1. Group 3, *rnr1* alleles (*rnr1-D226G/V/N*, *rnr1-S242T, rnr1-R256H, Y779C, rnr1-G267C* and *rnr1-S269P*) that interact with proofreading defective DNA polymerase alleles and a *msh2Δ* mutation, cause a strong mutator phenotype (*CAN1* inactivation) in the absence of Exo1, but do not show a frameshift mutator phenotype in the presence of Exo1. Group 4, *rnr1* alleles (*rnr1-K243E, rnr1-I262T,M275I* and *rnr1-I262V,N291D*) that interact with DNA polymerase proofreading defective alleles and a *msh2Δ* mutation, cause strong mutator phenotype in the *CAN1* assay but in addition they show increased frameshift mutations in an *EXO1*-WT background (Supplementary Figure S1). Within groups 3 and 4, we identified a subset of *rnr1* alleles (*rnr1-D226G/V/N, rnr1-R256H, Y779C, rnr1-S269P* and *rnr1-I262T,M275I*) that caused survival/growth defects in the absence of Rnr3 or Dun1 (Table 2 and Supplementary Figure S2B). The Rnr3-dependency indicates that these *rnr1* mutations are severely compromising Rnr1 enzymatic activity, such that cells rely on Rnr3 for dNTP production.

Interestingly, all *rnr1* mutations resulting in GD/SL in an *msh2Δ* background caused similar growth defects in DNA polymerase proofreading defective backgrounds (*pol2-04* and *pol3-01*). The reciprocal correlation did not hold true for those mutations causing GD/SL in *pol2-04* and *pol3-01* mutant backgrounds, as they either caused (groups 3 and 4) or not (group 2) GD/SL in the absence of Msh2. These observations indicate that the correction of DNA replication errors associated to changes in dNTPs have distinct requirements in regard of DNA polymerase proofreading and/or MMR, depending on the type of dNTP alteration.

rnr1 mutations resulting in increased mutagenesis cause either elevated or imbalanced dNTP pools

To test the assumption that mutator phenotypes in strains carrying *rnr1* mutations resulted from dNTP pool alterations, we quantified rNTP and dNTP levels in strains complemented by mutant *rnr1* plasmids, as previously reported (11). We focused our analysis on those *rnr1* alleles causing moderate or strong mutator phenotype in the *exo1Δ* background, resulting in at least a 5-fold increase in the *CAN1* inactivation rate, or at least 40- or 150-fold increase in the *hom3-10* or *lys2-10A* frameshift reversion assays, respectively. These different selected thresholds, though arbitrary, aim to take into consideration the distinct linear dynamic range of these three mutator assays. In agreement with the role of Rnr1 downstream of rNDP biosynthesis, *rnr1* mutations did not cause major changes in rNTPs (Supplementary Table S1); however, all mutations resulted in either an overall increase in dNTP concentrations or a dNTP pool imbalance (Figure 2A and Supplementary Table S2). Rnr1 mutant alleles were sorted according to their genetic interactions (GD/SL) and mutator phenotypes (Table 2). Among *rnr1* alleles in group 1, *rnr1-F15S* is the only identified mutation predicted to affect Rnr1's A-site, and in contrast to other identified mutations, it is the only mutation that resulted in an overall increase in dNTPs (on average, 6.5 over WT levels) without affecting dNTP ratios. All remaining mutations clustered within amino acids 226–291, a region that forms part of the S-site, and resulted in different dNTP imbalances, characterized by having either two or three dNTPs with increased concentrations relative to WT levels. Among them, some caused a reduction in dATP (e.g. *rnr1-S242T* or *rnr1-G267C*) or dATP and dGTP levels (e.g. *rnr1-A245V*) relative to WT levels. Furthermore, all *rnr1* mutations resulted in increased pyrimidine levels; having a relatively constant dCTP/dTTP ratio (ranging from 0.9- to 1.6-fold) but fluctuating dGTP/dATP ratio (ranging from 0.6- to 13.4-fold) mainly determined by changes in dGTP concentrations (Figure 2A and Supplementary Table S2). Taken together, these results indicate that the mutator phenotypes linked to these *rnr1* mutant alleles are caused by either increased or imbalanced dNTP pools.

To further explore the potential association between GD/SL and changes in dNTP pools, we analyzed dNTP pool alterations in more detail by plotting the log2 of the normalized ratio of dGTP to pyrimidine levels over % of dATP levels (Figure 2B). In this way, *rnr1* mutations resulting in an equal increase in dGTP and pyrimidine levels are on the x-axis ($y = 0$), whereas *rnr1* mutations causing high dGTP or high pyrimidine levels are above ($y > 0$) and below ($y < 0$) the x-axis, respectively. All *rnr1* mutations but one (*rnr1-F15S*) resulted in lower relative dATP abundance (% dATP/total dNTP) compared to WT (Figure 2B, x-axis). Strikingly, *rnr1* mutations that interact exclusively with proofreading-defective polymerases (group 2, Figure 2B marked in blue), all showed at least 4-fold increased pyrimidine levels over dGTP ($y < -2$). In contrast, *rnr1* mutations causing GD/SL in both proofreading- and MMR-deficient backgrounds (group 3 and group 4) clustered in a region confined to $\leq$12% dATP and a dGTP/(dCTP+dTTP) ratio $\geq$ 0.25 (normalized to WT). *Rnr1* mutant alleles in group 3 and group 4 resulted in a similar type of dNTP imbalance characterized by elevated dCTP, dTTP and dGTP levels, and close to WT dATP level. However, in contrast to group 3, *rnr1* mutant alleles in group 4 presented in general higher dGTP levels and caused a frameshift mutator phenotype in an *EXO1*-WT background (Supplementary Figure S1). One exception was *rnr1-G267C* allele that caused a dNTP imbalance remarkably similar to *rnr1-I262T,M275I,* but did not cause an increased mutator phenotype in the Exo1-WT strain background (Supplementary Figure S1). One possible explanation for this discrepancy may be due to potential differences in cell cycle progression triggered by dNTP limitations that may affect dNTP concentrations and consequently our interpretations.

dNTP limitation threshold triggers S-phase checkpoint

Based on the above-mentioned characterization we selected seven from the here identified *rnr1* alleles, as well as the

Table 2. Summary of *rnr1* mutant alleles identified in this study including synthetic growth defect/lethal interactions and mutator phenotypes

Allele*	Synthetic growth defect/lethality			*CAN1* mutator phenotype in *exo1Δ*[1]	Frameshift mutator phenotype in *EXO1*-WT[2]
	pol3-01	*pol2-04*	*msh2Δ*		
Group 1 (no interaction or just with *pol3-01*)					
rnr1-G8D,V278A	-	-	-	Weak	-
rnr1-F15S	-	-	-	Strong	-
rnr1-I231T,T244A	-	-	-	Weak	-
rnr1-T244I,V278A	SL	-	-	Moderate	-
rnr1-I262V	-	-	-	Weak	-
rnr1-T265A	GD	-	-	Weak	-
rnr1-P274L	GD	-	-	Weak	-
rnr1-M275T	-	-	-	Weak	-
rnr1-T282A	-	-	-	Weak	-
rnr1-T282S	-	-	-	Weak	-
rnr1-A283V,S425L	SL	-	-	Weak	-
Group 2 (interaction with *pol2-04* and *pol3-01*)					
rnr1-A245V	SL	GD	-	Moderate	-
rnr1-G271S	SL	GD	-	Weak	-
rnr1-Y285C	SL	GD	-	Moderate	-
Group 3 (interaction with *pol2-04*, *pol3-01* and *msh2Δ*)					
rnr1-D226G‡	GD	GD	GD	Strong	-
rnr1-D226V‡	GD	GD	GD	Strong	-
rnr1- D226N‡,*S117P*†	GD	GD	GD	Strong	-
rnr1-S242T	SL	GD	GD	Strong	-
rnr1-R256H, Y779C‡	SL	GD	GD	Strong	-
rnr1-G267C	SL	GD	GD	Strong	-
rnr1-S269P‡	SL	GD	GD	Strong	-
Group 4 (interaction with *pol2-04*, *pol3-01* and *msh2Δ* and mutator in *EXO1*-WT)					
rnr1-K243E	SL	GD	GD	Strong	Mutator
rnr1-I262T,M275I‡	SL	GD	GD	Strong	Mutator
rnr1-I262V,N291D	SL	GD	GD	Strong	Mutator

*Indicated allele expressed on a low-copy number plasmid was used for complementation studies in strains lacking the chromosomal *RNR1* gene in addition to the indicated mutations. Passenger mutations are marked with †. '-' indicates growth similar to WT-*RNR1*; 'GD', growth defect; 'SL', synthetic lethality.
‡*rnr1* alleles show GD or SL in the absence of *RNR3* and *DUN1*.
[1]Mutator phenotype according to the *CAN1* inactivation rate (Table 1) fold increase over *WT-RNR1* (in *rnr1Δ exo1Δ*): 2–5 = weak; 6–10 = moderate; ≥ 11 = strong.
[2]Frameshift mutator phenotype (*lys2-10A* assay) in *EXO1*-WT *rnr1Δ* background (Supplementary Figure S1B).

previously reported *rnr1-D57N* mutation that results in an overall increase in dNTP pools (34) for integration at the *RNR1* chromosomal locus in both WT and *exo1Δ* strains. Within group 1, we selected *rnr1-F15S* as this allele causes a strong *exo1Δ*-dependent mutator phenotype, and similar to *rnr1-D57N* mutant, results in an overall increase in dNTPs (Figure 2A). Mutants within group 2 presented a dNTP imbalance characterized by having elevated two out of the four dNTPs ('*2 out of 4*' dNTP imbalance). Within this group, we chose *rnr1-A245V* and *rnr1-Y285C*, as both caused a stronger *exo1Δ*-dependent mutator phenotype compared to *rnr1-G271S* (Tables 1 and 2). In contrast, mutants in group 3 had in common a '*3 out of 4*' dNTP imbalance, characterized by increased dCTP, dTTP and dGTP levels and relatively low dATP. From this group, we selected one Rnr3-dependent (*rnr1-R256H, Y779C*) and one Rnr3-idenpendent allele (*rnr1-S242T*), both of which resulted in a strong *exo1Δ*-dependent mutator phenotype (Tables 1 and 2). Mutants within group 4, had a similar '*3 out of 4*' dNTP imbalance (group 3), but with the distinction that these alleles had in general higher dGTP levels ('*3 out of 4 with extra-high dGTP*'). From group 4, we selected alleles *rnr1-K243E* and *rnr1-I262V,N291D* that showed the highest dGTP levels for integration at the chromosomal locus. In case of the *rnr1-K243E* mutation, we succeeded in introducing this mutation at the chromosomal locus in the WT background but not in an *exo1Δ* strain.

Analysis of the dNTP levels in strains carrying *rnr1*-integrated mutant alleles (Figure 3A and Supplementary Table S3) revealed strong similarities to strains carrying corresponding plasmid-borne alleles (Figure 2A and Supplementary Table S2). However, in case of *rnr1-R256H, Y779C* we noticed a less pronounced increase in dNTP pools, likely as result of the lower Rnr1-expression levels reached with chromosomally-integrated alleles.

Mutations causing severe dNTP limitations have been associated with S-phase checkpoint activation and synthetic lethality in a *rnr3Δ* background (11). As *rnr1-R256H, Y779C* mutant allele caused synthetic lethality in an *rnr3Δ* background (Table 2 and Supplementary Figure S2B), we anticipated that this mutation could show constitutively active S-phase checkpoint. In agreement with this, strains expressing the *rnr1-R256H, Y779C* allele exhibited a higher percentage of cells in S phase (Figure 3B), and in-

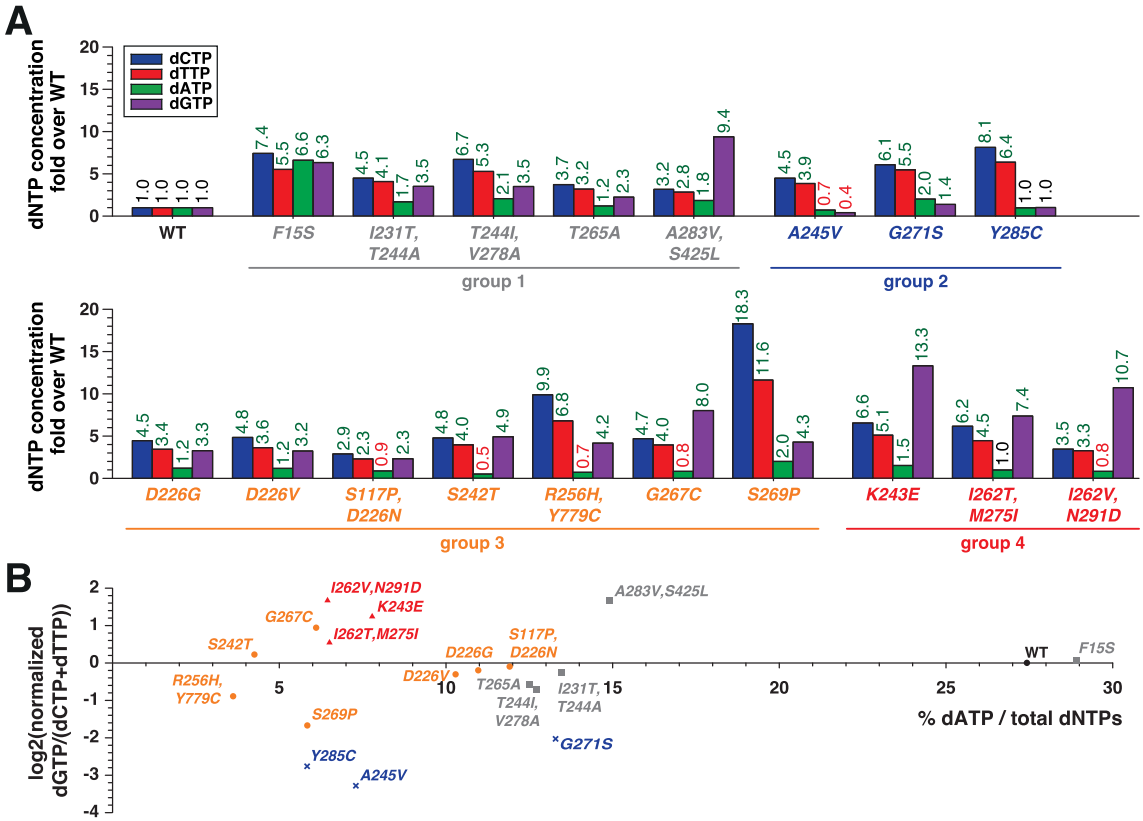

Figure 2. *rnr1* mutations cause imbalanced or increased dNTP pools. (**A**) Quantification of dNTP levels by HPLC in *rnr1Δ* strains complemented by mutant *rnr1* plasmids. dNTP concentrations are expressed relative to the WT levels. Numbers on top indicate the fold increase (in green) or decrease (in red) in dNTP pools over WT. (**B**) Graphical representation of the relative percentage of dATP over the total dNTPs (% dATP / total dNTPs) over the $\log_2$ dGTP/(dCTP+dTTP) normalized to WT levels for strains shown in A. To correlate dNTP levels with the mutator phenotype and the genetic interactions resulting in synthetic growth defects or lethality, the identified mutations were clustered in four groups: mutations indicated by the grey squares did not cause genetic interactions (or just with *pol3-01*) (group 1). Mutations highlighted as blue crosses caused growth defects in both DNA polymerase proofreading defective backgrounds (*pol3-01* and *pol2-04*) (group 2). Mutations indicated as orange circles (group 3) and red triangles (group 4) not only presented growth defects in DNA polymerase proofreading defective backgrounds but also in a MMR-deficient background (*msh2Δ*), with the distinction that mutant alleles in group 4 have an increased mutator phenotype in an *EXO1*-WT background. See Table 2 and Supplementary Figure S2 for genetic interactions and Supplementary Figure S1 for mutator phenotypes in an Exo1-WT background.

creased Rnr1-4 subunits expression levels (Figure 3B and C), which is indicative of DNA damage checkpoint activation (35). Interestingly, the *rnr1-A245V* allele that did not interact with *rnr3Δ* mutant, also caused S-phase checkpoint activation, albeit less severe (about twice more cells in S-phase and increased expression of Rnr1–4 subunits, relative to WT) (Figure 3B and C). In agreement with a previous report (11), *rnr1* mutations causing constitutive activation of S-phase checkpoint (*rnr1-A245V* and *rnr1-R256H, Y779C*) correlated with reductions in at least one dNTP (relative to WT). Nevertheless, we observed that small reductions in dATP levels (up to 20%) did not trigger S-phase checkpoint activation (e.g. *rnr1-S242T* or *rnr1-Y285C*) (Figure 3A–C and Supplementary Table S3B). These results indicate that the activation of the S-phase checkpoint in budding yeast responds to a dNTP limitation threshold, and not to increased dNTP pool size or the accumulation of mutations.

Interestingly, *rnr1-K243E* and *rnr1-I262V,N291D* alleles caused a moderate increase in Rnr3 expression (and also Rnr4 in case of *rnr1-K243E*) without having evident dNTP limitations or an S-phase delay. At this point we can speculate that the extremely high dGTP concentrations (dGTP levels correspond to ∼50% of GTP concentration in WT cells) may potentially interfere with some cellular processes that occur prior to G1 phase transition. For example, previous studies *in vitro* have shown that dGTP supports tubulin nucleation even more efficiently than GTP (36). Thus, increased dGTP levels may potentially interfere with microtubule dynamics, which could influence chromosome segregation.

rnr1 mutations at the endogenous genomic locus induce mutagenic dNTP alterations

Next, we determined mutation rates in strains carrying *rnr1*-integrated alleles in the WT and *exo1Δ* strains. In agreement with results obtained with plasmid-borne alleles, all *rnr1*-integrated alleles caused a synergistic increase in the mutation rate in an *exo1Δ* mutant (Table 3). Among the tested alleles, *rnr1-F15S* mutation affected the A-site and caused an overall increase in the dNTP pool, rather than an imbalance. As previous reports have described one mu-

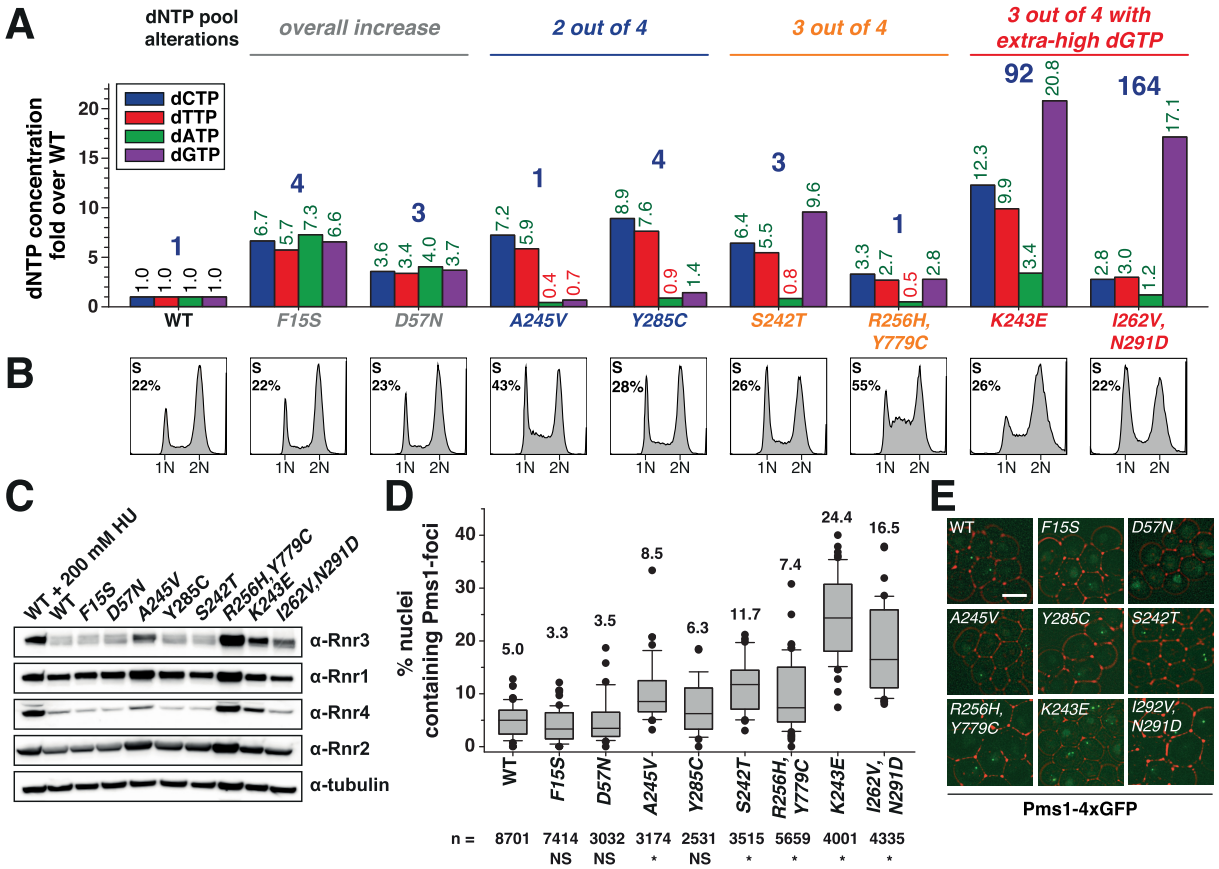

Figure 3. *rnr1* mutations integrated at the endogenous genomic locus result in dNTP pool alterations, S-phase checkpoint activation and increased Pms1-foci abundance. (**A**) Quantification of dNTP levels in indicated strains. dNTP concentrations are indicated relative to WT levels. Numbers of top in green and red indicate the fold increase/decrease in dNTP pools. Numbers in blue indicate the fold increase in the *CAN1* mutation rate determined for each *rnr1* mutant strain in an *EXO1*-WT background (see Table 3). The *rnr1* mutants were classified into four groups according to their dNTP alterations, genetic interactions (GD/SL) and mutator phenotype. (**B**) DNA content analysis and percentage of cells in S phase of the indicated strains. (**C**) Whole-cell lysates of yeast strains expressing *rnr1* alleles analyzed by western blotting with antibodies recognizing Rnr1–4 subunits. Tubulin was used as loading control. (**D**) Quantification of Pms1-4xGFP nuclear foci (as percentage) in strains expressing WT or mutant *rnr1* mutant alleles. Data is presented in box-plots with whiskers (indicating the 25th and 75th percentiles) and dots representing outliers. Numbers on top of the box-plots correspond to the median of three independent experiments. * Denotes *rnr1* alleles causing a significant increase ($P < 0.005$) in the abundance of cells containing Pms1-foci. 'NS' indicates not significantly different. Total number of imaged cells ($n =$) are indicated. (**E**) Representative images of Pms1-4xGFP foci in strains containing the indicated *rnr1* allele. Scale bar represents 5 μm.

tation that prevents the allosteric inhibition by dATP (*rnr1-D57N*) (Figure 1E) (34,37,38) we compared side-by-side the effects of these two mutations *in vivo*. As previously reported (34), *rnr1-D57N* mutation resulted in a modest mutator phenotype in the *CAN1* assay (3-fold higher than WT) (Table 3), which was comparable to the effect of *rnr1-F15S* mutation. Interestingly, *rnr1-F15S* mutation, but not *rnr1-D57N*, resulted in a synergistic increase in the mutation rate in an *exo1Δ* background (7-, 83- and 13-fold higher than *exo1Δ* in the *CAN1*, *hom3-10* and *lys2-10A* assays, respectively) (Table 3). While the lack of a synergistic mutator interaction for *rnr1-D57N* allele and *exo1Δ* was unexpected, it may correlate with its weaker increase in dNTP levels (on average 3.7-fold over WT) compared to *rnr1-F15S* (on average 6.6-fold over WT) (Figure 3A).

Based on the reported human RNR structure (39), Phe15 is predicted to be located at the interface formed by two dATP-bound cones from adjacent Rnr1 dimers (illustrated in Figure 1E). This study showed that mutagenizing the adjacent residue, Asp16 (*rnr1-D16R*), disrupted the dATP-dependent RNR hexamerization *in vitro*, resulting in mutant complexes that do not respond to dATP inhibition (39). Most likely similar to the *rnr1-D16R* mutation (39), the *rnr1-F15S* mutation may disrupt the formation of dATP-dependent hexamers, making Rnr1 refractory to dATP inhibition.

Despite the fact that most chromosomally integrated *rnr1*-mutant alleles caused moderate or high mutation rates (up to 10^{-4} mutations per cell division in frameshift reversion assays) when expressed in an *exo1Δ* background, the majority failed to do so in an *EXO1*-WT background (Table 3). Two exceptions were *rnr1* alleles: *rnr1-K243* and *rnr1-I262V,N291D* that when integrated at the *RNR1* locus, consistent with results obtained after expression in a low-copy number plasmid (Supplementary Figure S1), caused high mutation rates even in the presence of *EXO1* (Table 3). Re-

Table 3. Mutation rates caused by *rnr1* mutations integrated at the *RNR1* genomic locus in Exo1-proficient and Exo1-deficient backgrounds

	Mutation rate (fold increase)*		
Relevant genotype	Can^R	Thr^+	Lys^+
WT	8.7 [7.2–10.0] × 10^{-8} (1)	2.0 [1.1–3.0] × 10^{-9} (1)	2.1 [1.8–2.3] × 10^{-8} (1)
exo1Δ	7.4 [6.3–9.8] × 10^{-7} (9)	8.7 [6.1–15.0] × 10^{-9} (4)	1.4 [0.9–1.8] × 10^{-7} (7)
msh2Δ	5.4 [4.4–7.2] × 10^{-6} (61)	6.4 [5.2–12.9] × 10^{-6} (3211)	9.9 [8.1–10.8] × 10^{-5} (4762)
'overall increased'			
rnr1-F15S	3.5 [2.8–4.2] × 10^{-7} (4)	5.3 [4.4–7.6] × 10^{-9} (3)	2.0 [1.6–2.6] × 10^{-8} (1)
rnr1-F15S exo1Δ	5.1 [3.9–6.3] × 10^{-6} (59)	6.5 [4.0–8.9] × 10^{-7} (330)	1.9 [1.3–2.3] × 10^{-6} (93)
rnr1-D57N	2.2 [2.0–3.7] × 10^{-7} (3)	4.0 [2.5–7.5] × 10^{-9} (2)	1.6 [1.3–2.3] × 10^{-8} (1)
rnr1-D57N exo1Δ	6.5 [4.0–9.1] × 10^{-7} (7)	1.6 [1.2–1.8] × 10^{-8} (8)	4.6 [3.5–6.4] × 10^{-8} (2)
'2 out of 4'			
rnr1-A245V	1.1 [0.8–1.4] × 10^{-7} (1)	3.1 [2.1–4.2] × 10^{-8} (16)	3.8 [2.2–5.3] × 10^{-8} (2)
rnr1-A245V exo1Δ	2.0 [1.1–3.7] × 10^{-6} (22)	1.1 [0.6–2.1] × 10^{-5} (5405)	1.3 [0.8–3.1] × 10^{-5} (634)
rnr1-Y285C	3.2 [1.8–5.1] × 10^{-7} (4)	4.8 [3.7–8.7] × 10^{-8} (24)	1.6 [0.9–2.0] × 10^{-7} (8)
rnr1-Y285C exo1Δ	1.6 [1.1–3.2] × 10^{-5} (184)	4.6 [3.0–7.8] × 10^{-5} (23037)	1.9 [1.6–5.5] × 10^{-4} (9139)
'3 out of 4'			
rnr1-S242T	2.6 [2.0–5.1] × 10^{-7} (3)	1.6 [1.1–3.1] × 10^{-8} (8)	1.3 [0.8–2.7] × 10^{-7} (6)
rnr1-S242T exo1Δ	2.4 [1.9–4.0] × 10^{-5} (273)	9.4 [5.8–18.5] × 10^{-6} (4743)	1.7 [1.3–3.0] × 10^{-4} (8017)
rnr1-R256H, Y779C	9.5 [7.1–16.0] × 10^{-8} (1)	2.6 [1.4–4.0] × 10^{-8} (13)	9.2 [7.2–11.6] × 10^{-8} (4)
rnr1-R256H, Y779C exo1Δ	2.2 [1.5–3.3] × 10^{-6} (25)	3.2 [2.1–3.2] × 10^{-6} (1619)	7.3 [5.4–8.8] × 10^{-6} (351)
'3 out of 4 with extra-high dGTP'			
rnr1-K243E	8.1 [4.4–11.3] × 10^{-6} (92)	1.5 [1.1–2.4] × 10^{-5} (7362)	2.7 [2.0–4.6] × 10^{-5} (1319)
rnr1-K243E exo1Δ†	nd	nd	nd
rnr1-I262V,N291D	1.4 [0.9–2.4] × × 10^{-5} (164)	5.4 [3.8–8.3] × 10^{-6} (2731)	6.7 [4.5–10.8] × 10^{-5} (3216)
rnr1-I262V,N291D exo1Δ	4.3 [3.1–7.1] × 10^{-5} (489)	1.9 [0.7–3.0] × 10^{-5} (9366)	2.1 [0.9–3.4] × 10^{-4} (10103)

*Median rates of inactivation of *CAN1* gene (Can^R) and *hom3-10* (Thr^+) and *lys2-10A* (Lys^+) frameshift reversion, with 95% confidence interval in square brackets and fold increase relative to WT strain in parentheses. Strains with partial or total loss of mismatch repair activity (*exo1Δ* and *msh2Δ*, respectively) were included as reference.
†Despite several attempts we could not obtain this double mutant strain. 'nd' indicates 'not determined'.

markably, both mutant alleles shared a common type of dNTP imbalance, in which three out of the four dNTPs were elevated, with under-represented dATP concentrations and very high dGTP levels (21- and 17-fold over WT, respectively) ('*3 out of 4 with extra-high dGTP*'). These observations suggest that among the four types of dNTP alterations here investigated, the '*3 out of 4 with extra-high dGTP*' imbalance correspond to the most detrimental dNTP pool alteration for DNA replication fidelity. In addition, these observations indicate that in the context of a '*3 out of 4*' type of imbalance, increased dGTP levels inversely correlate with DNA replication fidelity.

Replication errors induced by a '*3 out of 4 with extra-high dGTP*' dNTP imbalance frequently escape DNA polymerase proofreading resulting in increased Pms1-foci abundance

We have previously shown that the MMR complex Mlh1-Pms1 forms nuclear foci that mark active sites of MMR in living yeast cells (19,40). Accordingly, MMR mutants with defects downstream mispair recognition (e.g. during nicking or excision steps) or strains with reduced DNA replication fidelity (e.g. proofreading defective or active-site DNA polymerase mutants) showed increased Pms1-foci abundance (19). As the mutation rate does not reflect the total number of replication errors, but rather the fraction that escaped correction, we quantified the abundance of Pms1-foci in strains expressing chromosomally integrated *rnr1* mutant alleles (and a fluorescently-tagged Pms1 gene (Pms1-4xGFP)). Mutant alleles *rnr1-F15S, rnr1-D57N* and *rnr1-Y285C* did not cause a significant increase in the percentage of cells containing Pms1-foci relative to the WT (Figure 3D and E). Mutations *rnr1-A245V, rnr1-S242T* and *rnr1-R256H, Y779C* resulted in a mild but significant increase in the percentage of cells containing Pms1-foci (Mann–Whitney test, $P < 0.005$). In contrast, mutations *rnr1-K243E* and *rnr1-I262V,N291D* caused the strongest increase in Pms1-foci abundance (4.9- and 3.3-fold over WT, respectively) (Figure 3D and E) (Mann–Whitney test, $P < 0.005$), similar as previously reported for strains with compromised DNA polymerase replication fidelity (19).

These results indicate that among the four types of dNTP alterations here evaluated, only *rnr1* mutations resulting in a '*3 out of 4 with extra-high dGTP*' dNTP imbalance, are causing a considerable number of replication errors that escape DNA polymerase proofreading function, leading to increased Pms1 repair foci abundance. These results are in agreement with the Exo1-independent mutator phenotype observed in *rnr1Δ* strains complemented with these mutant alleles (Supplementary Figure S1).

A '*3 out of 4*' dNTP imbalance overwhelms DNA polymerase proofreading and MMR function resulting in base substitutions and frameshift deletions

The synthetic GD/SL interactions between *rnr1* mutant alleles resulting in either a '*3 out of 4*' or a '*3 out of 4 with extra-high dGTP*' imbalance and the *msh2Δ* mutation (Table 2 and Supplementary Figure S2), suggest that in the absence of MMR, these double mutant combinations accumulate a large number of mutations compromising cell viability. As insertions or deletions are in general more deleterious than base substitutions, we asked whether these previously mentioned imbalances are causing more frequently frameshift mutations than a '*2 out of 4*' imbalance. For this, we performed mutational spectra analysis at the *CAN1* locus in strains carrying chromosomally-integrated *rnr1-Y285C*, *rnr1-R256H,Y779C* and *rnr1-I262V,N291D* alleles (Figure 4A and Supplementary Table S4), representing the three types of dNTP imbalances here characterized. Mutational spectrum in *rnr1-Y285C* revealed a 7- and 4-fold increase in A:T to C:G and A:T to T:A transversions, respectively, relative to WT (17). Outstandingly, together these transversions accounted for 50% of all *CAN1* inactivating mutations, which are likely promoted by the slightly reduced dATP and excessively high concentrations of dCTP and dTTP. Further analysis revealed mutational hotspots A538C and A680T, both of which occurred 10-times more frequently than in a WT strain (Figure 4B and Supplementary Table S5). All three mutational hotspots are in agreement with the relatively low dATP and high concentrations of dCTP and dTTP (Figure 3A), which may facilitate A to C/T transversions.

In contrast, strains carrying *rnr1-R256H*,*Y779C* or *rnr1-I262V*,*N291D* mutations presented less base substitutions but more frameshift mutations (mainly A/T deletions) compared to WT mutation spectrum (Supplementary Table S4). Remarkably, in the *rnr1-I262V*,*N291D* mutant strain, the frequency of frameshift mutations (82%) strongly resembled that of MMR deficient strains (about 85% frameshift mutations) (24,41). However, in contrast to the latter, in which frameshift deletions (but also insertions) were found at several mononucleotide runs within the *CAN1* gene, the *rnr1-I262V*,*N291D* presented mainly one mutational hotspot at position 964–969, involving the deletion of a A:T base pair in a six A:T mononucleotide run (Figure 4C and Supplementary Table S5). Strikingly, deletions at this single hotspot accounts for 66% of the overall mutation rate associated with *rnr1-I262V*,*N291D* mutation. These results indicate that this specific dNTP imbalance strongly favors frameshift deletion events at this specific hotspot, which frequently escape MMR correction. As the mutational spectra is largely influenced by the sequence context, we used an alternative mutational reporter (*URA3* gene) to further validate the mutational signature caused by *rnr1-I262V*,*N291D* allele. The *URA3* spectrum caused by *rnr1-I262V*,*N291D* mutant allele showed a 10% reduction in base pair mutations and a 2-fold increase in single nucleotide A/T deletions, compared with the reported WT *URA3* spectrum (42). Similar to the *CAN1* mutation spectra, base substitutions in *URA3* were mainly A:T to G:C transitions, which occurred 27-times more frequently than in the WT strain (Figure 4D and Supplementary Table S6). On the other hand, frameshifts were mostly located at regions containing 3–4 mononucleotide runs, probably due to the low number of longer mononucleotide repeats within *URA3* gene.

In summary, we found that a '*3 out of 4*' type of dNTP imbalance represents the most mutagenic type of dNTP pool alteration that favors not only base substitutions, but also single nucleotide deletion events, mainly at mononucleotide runs where the under-represented dNTP is on demand during DNA synthesis. This mutagenic potential is likely driven by a combinatorial effect: first, the under-represented dNTP favors single nucleotide deletions or base substitutions; and second, the other three dNTPs which are in excess diminish the effectiveness of the DNA polymerase proofreading by promoting mispair/frameshift extension driven by the 'next-nucleotide effect' (43,44). According to this model, after misincorporation of a nucleotide (or a slippage event), the high concentration of the next nucleotide to be incorporated, will favor its incorporation instead of mismatch proofreading. In the presence of a '*3 out of 4*' dNTP imbalance, the synthesis of mononucleotide runs demanding the under-represented nucleotide pool, will lead to a frameshift deletion that will frequently escape DNA polymerase proofreading, given that after the mononucleotide run any upcoming nucleotide will be highly abundant. Thus, under this extreme type of dNTP imbalance the sequence context becomes irrelevant for mismatch extension, though it might have important consequences on how efficiently a specific mutation/frameshift is recognized by MMR (45–47).

DISCUSSION

Here, we have screened for mutations in yeast *RNR1* gene that cause increased mutagenesis in an *exo1Δ* mutant background. We identified 24 *rnr1* mutant alleles either associated with an overall increase in dNTP concentrations or changes in dNTP ratios (balance). Most mutations caused dNTP pool imbalances and clustered in or near the allosteric S-site but were not restricted to loop 2, whereas one mutation causing an increase in dNTP pool size was located at the allosteric A-site. All mutations resulting in constitutive S-phase checkpoint activation and synthetic lethality in an *rnr3Δ* background presented one or two limiting dNTPs (with concentrations below WT levels). Our data suggest that cells respond to a dNTP limitation threshold; reductions of 10–20% in dATP levels are well tolerated; however, higher reductions (≥50%) triggered activation of the S-phase checkpoint. Interestingly, a 50% reduction in dATP levels results in dATP concentrations comparable to dGTP levels in a WT strain (Supplementary Table S2 and Supplementary Table S3B), suggesting that the dNTP limitation threshold value approaches WT-dGTP levels, which has the lowest concentration among all four dNTPs in yeast but also in mammalian cells (48,49).

One important aspect of this *RNR1* random mutagenesis screen is that is not restricted *a priori* for a specific Rnr1 protein domain, hence allowing the unbiased identification of mutations with profound effects on dNTP homeostasis. Moreover, given our plasmid shuffling complementation-

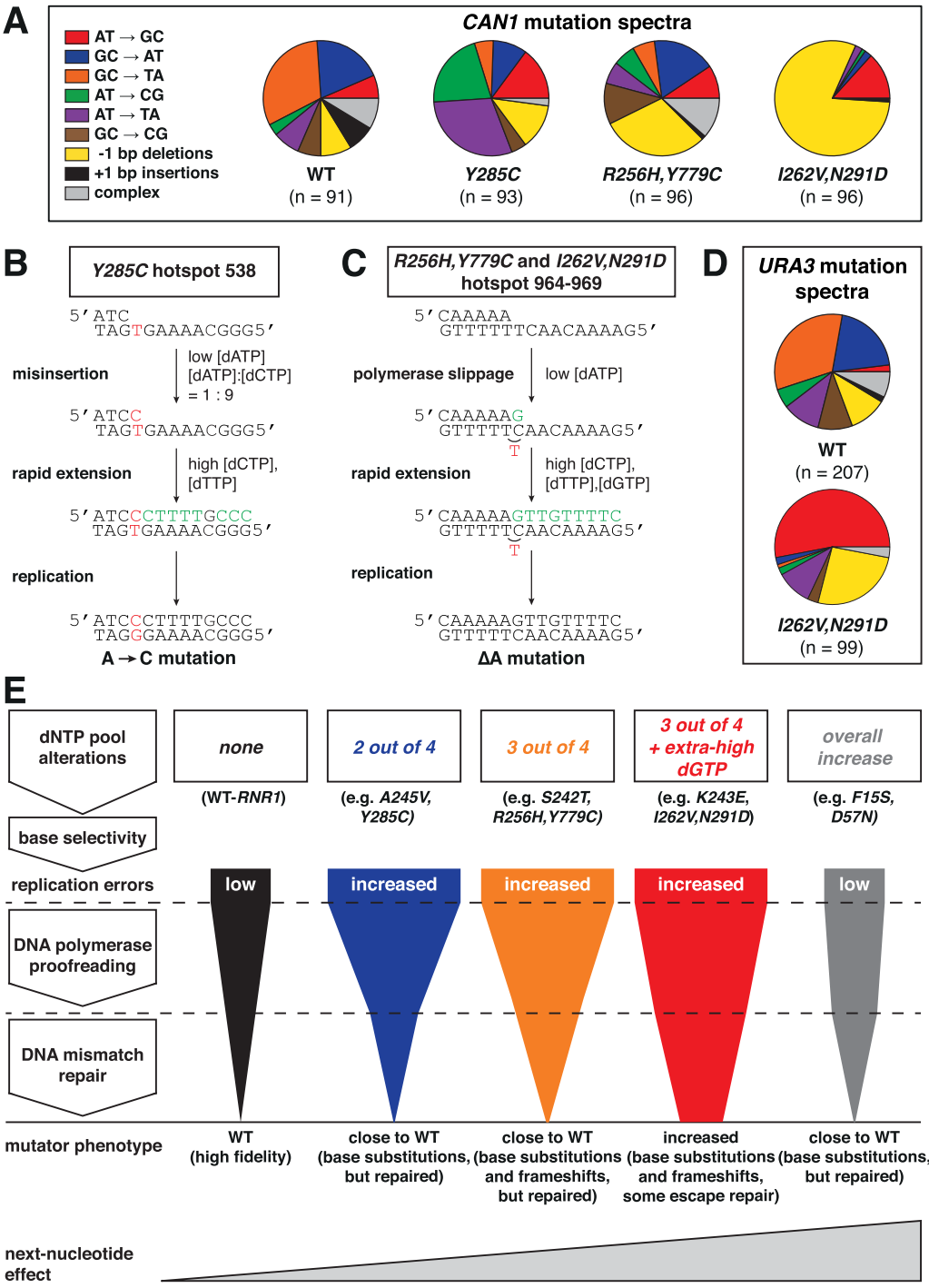

Figure 4. Mutation spectra analysis revealed highly mutagenic dNTP imbalances that escape DNA polymerase proofreading and MMR. (**A**) *CAN1* mutation spectrum in WT (17) and indicated strains expressing *rnr1* mutant alleles. Independent Can^R clones ($n \geq 91$ per genotype) were sequenced for *CAN1* mutations. Graphs indicate the relative distribution of identified mutations (see also Supplementary Table S4 and Supplementary Table S5). (**B**) *CAN1* mutational hotspot (A538C) frequently associated to *rnr1-Y285C* mutation. Predicted mutation is noted in red. Nucleotides marked in green (immediately after the mutation) are facilitating mispair rapid extension prior proofreading, due to their higher abundance in strains expressing *rnr1* mutant alleles, compared to wild-type *RNR1*. (**C**) The -1A frameshift deletion hotspot (964–969) was frequently found in strains expressing *rnr1-R256H, Y779C* or *rnr1-I262V,N291D* mutant alleles. (**D**) *URA3* mutation spectrum in WT (42) and a strain expressing *rnr1-I262V,N291D* mutant allele (see also Supplementary Table S6). Mutation spectra were color-coded in the same way as in (A). (**E**) Distinct dNTP pool alterations differentially rely on DNA polymerase proofreading and MMR activity for mutation avoidance. The funnels below each of the different dNTP pool alterations represent DNA replication errors that are corrected by DNA polymerase proofreading and/or MMR. Genetic interactions between mutations resulting in specific dNTP alterations and mutations affecting DNA replication fidelity were color-coded as in Figure 2B. Among the four types of dNTP alterations, imbalances characterized by a '*3 out of 4 with extra-high dGTP*' result in increased DNA replication errors that frequently escape DNA polymerase proofreading and MMR.

based strategy (done in a Rnr1-deficient strain), all identified mutations resulted in mutant RNR complexes that had to retain substantial enzymatic activity in order to sustain cell viability. This approach overcomes certain limitations of mutations engineered by rational design, which in some cases (*rnr1-Q288A* and *rnr1-R293A*) led to extremely imbalanced dNTP pools and lethal phenotypes, unless these alleles were overexpressed or integrated in the presence of a repressed WT-*RNR1* gene (11,50).

Our *RNR1* mutagenesis screen shares some similarities to a previous screen that identified mutations in *NrdA* and *NrdB* ribonucleotide reductase genes in *E. coli* (13). Alike most *RNR1* mutations reported here, mutations in *NrdA* located either at the A-site or at the S-site, and resulted in increased and imbalanced dNTP pools, respectively. Despite some protein sequence conservation between *S. cerevisiae* and *E. coli RNR* (29% protein identity), none of the *RNR1* mutated residues identified here were previously found in *E. coli NrdA*. This observation was unexpected, as several of *RNR1* mutations (e.g. *rnr1-D226G, rnr1-I231T, rnr1-R256H, rnr1-I262V, rnr1-G271S*, *rnr1-P274L*, among others) identified in our screen are affecting conserved residues between both species. In part, this might be due to technical differences between both screening approaches, including the use of a 'sensitized mutator background' (*exo1Δ*), random mutagenesis procedures, mutational reporters, etc.

Encouraged by the finding that specific mutations in *NrdB* gene (encoding the small RNR subunit in *E. coli*) resulted in dNTP imbalances (13), we performed a similar screen as described here for *RNR1,* in which we mutagenized the *RNR2* gene, encoding the yeast small RNR subunit, homolog of *E. coli NrdB*. In contrast to these previous findings, we could not identify *RNR2* mutations resulting in mutator phenotypes (data not shown). The absence of homolog mutator mutations in yeast *RNR2* may reflect structural differences and distinct regulatory requirements that may distinguish *E. coli* from *S. cerevisiae* RNR.

Intriguingly, all mutant alleles resulting in dNTP imbalances presented a lower relative percentage of dATP over the total dNTP pool (Figure 2B). This commonality might be in part linked to the frameshift reporters (*lys2-10A* and *hom3-10*) used for mutator phenotype identification (in addition to the general mutator assay based on *CAN1* inactivation). Low dATP concentrations may facilitate single deletion events at the 10 A:T and 7 T:A mononucleotide hotspot present in *lys2-10A* and *hom3-10*, respectively. On the other hand, low dTTP levels could have triggered a similar effect, although this type of imbalance was not observed. The absence of *rnr1* mutations resulting in low dTTP levels might be due to the compensatory effect of dCMP deaminase that converts dCMP into dUMP, which is then used for dTTP production (48,51). Additionally, as dATP acts as a RNR inhibitor, we speculate that high dATP levels might be incompatible with severely imbalanced dNTP pools independently of an activated S-phase checkpoint (e.g. *rnr1-S242T* and *rnr1-Y285C*).

rnr1 mutations interfering with A-site allosteric regulation

We found that *rnr1-F15S* causes a mild mutator phenotype driven by an increase in dNTP pool size (6.5-fold higher concentration of each dNTP over WT levels). Interestingly, *rnr1-F15S* mutation strongly interacted with *exo1Δ* resulting in 59-fold increase in *CAN1* mutation rate compared to WT (and about 7-fold higher than *exo1Δ*). Given the region affected by *rnr1-F15S* mutation, and supported by previous work by Dealwis group (39), we propose that *rnr1-F15S* mutation may prevent dATP-induced Rnr1 hexamerization, resulting in RNR mutant complexes that are refractory to dATP inhibition *in vivo*. Moreover, the finding that mutations causing elevated but balanced dNTP pools neither interact with proofreading-defective nor MMR-deficient mutants, suggest that elevated dNTP pools are in general less mutagenic than imbalanced dNTP pools. Thus, overall increased but balanced dNTP pools, do not result in a higher frequency of misincorporated nucleotides, but rather prevent DNA polymerase proofreading driven by the next-nucleotide effect. These replication errors that escape proofreading might be efficiently repaired by MMR (Figure 4E).

Two classes of mutations resulting in increased pyrimidine levels

Among the mutations that resulted in imbalanced dNTP pools *rnr1-A245V, rnr1-G271S* and *rnr1-Y285C*, had resulted in elevated pyrimidines and relatively low purine levels (Figures 2A and 3A). According to the *S. cerevisiae* Rnr1 crystal structure, the side chain of Tyr285 and the main chain (oxygen) of Gly271 both form a hydrogen-bond with a water molecule that interacts with the 2′-OH from the effector AMP-PNP (28). While these interactions may stabilize the binding of AMP-PNP (or ATP) at the S-site, similar interactions cannot take place with dNTP effectors. A previous study proposed that Tyr244 in *Salmonella typhimurium* (homolog residue of Tyr285 in yeast) hinders rNTP binding at the S-site because of a steric clash between the 2′-OH group of the ribonucleotide and the tyrosine side-chain (52). As rNTP concentrations in yeast cells are on average 50-times higher than dNTPs, one could predict that mutating Tyr285 will favor ATP binding at the S-site (the most abundant rNTP), which similar to dATP will promote CDP and UDP reduction (10,28). Supporting this hypothesis, replacing Tyr285 with less bulky residues (e.g. cysteine or alanine) or even phenylalanine (but to a lesser extent), favored pyrimidine production (this study and (11)). Based on our observations and previous findings, we propose that mutation of Tyr285 (and potentially also Gly271) largely abolishes the strong preference for dATP over ATP binding at the S-site, resulting in elevated pyrimidine levels driven by high intracellular ATP concentration.

The *rnr1-A245V* mutation, similar to *rnr1-Y285C,* resulted in increased pyrimidine levels but in addition caused a 60% and 30% reduction in dATP and dGTP levels, respectively. Given the proximity of Ala245 to the C-site, one could predict that replacing it with a bulky amino acid may decrease the substrate pocket size. Accordingly, the *rnr1-A245V* mutation may result in steric clashes that may favor the binding and reduction of pyrimidines over purines. Thus, we propose two alternative mechanisms that may explain the '*2 out of 4*' imbalance, either by abolishing the ability to discriminate rNTPs from dNTPs at the S-site (*rnr1-*

Y285C) or through mutations that may decrease the substrate pocket size (e.g. *rnr1-A245V*).

The tip of a mutational iceberg: the bad and the worst dNTP pool imbalance

In general, most identified *rnr1* mutations neither caused mutator phenotypes nor growth defects, unless they were expressed in DNA replication fidelity-compromised backgrounds. Thus, replication errors resulting from increased or imbalanced dNTP pools are in most cases proofread by DNA polymerases or corrected by MMR.

Genetic interactions between *rnr1* mutant alleles and mutations affecting DNA replication fidelity resulting in synthetic GD/SL (Table 2 and Supplementary Figure S2) revealed that overall increased dNTP pools are not affecting cell viability even in the absence of DNA polymerase proofreading function or MMR activity. In contrast, mutations resulting in specific dNTP imbalances relied for survival on DNA polymerase proofreading ('*2 out of 4*') or DNA polymerase proofreading and MMR ('*3 out of 4*' and '*3 out of 4 with extra-high dGTP*'). These findings are further supported by the *CAN1* mutation spectra analysis. For example, the *rnr1-Y285C* mutation that results in a '*2 out of 4*' imbalance presented a *CAN1* mutation spectrum dominated by base substitutions, which are favored by low dATP and high dTTP/dCTP concentrations (Figure 4A and Supplementary Table S4). On the other hand, *rnr1* mutations (*rnr1-R256H, Y779C* or *rnr1-I262V,N291D*) resulting in a '*3 out of 4*' or a '*3 out of 4 with extra-high dGTP*' dNTP imbalance, respectively, presented a high frequency of *CAN1* single nucleotide deletions (mainly A/T deletions) that are promoted by low dATP levels and the elevated concentrations of the remaining three dNTPs. Similar results were obtained in *rnr1-I262V,N291D* after analyzing the mutational spectrum in *URA3* gene (Figure 4D and Supplementary Table S6).

All together, these findings indicate that mutations causing '*2 out of 4*' type of imbalance result in base substitutions which are corrected to a large degree by DNA polymerase proofreading (Figure 4E). In agreement with this, *rnr1-Y285C* and *rnr1-A245V* mutants did not cause major increase in the abundance of Pms1-foci, which mark sites of DNA replication errors recognized by Mlh1-Pms1 MMR complex (Figure 3D and E).

Instead, mutations resulting in a '*3 out of 4 with extra-high dGTP*' imbalance cause frequent frameshift deletions and base substitutions that rely heavily on DNA polymerase proofreading and MMR for repair (Figure 4E). Accordingly, this imbalance caused increased abundance of Pms1-repair foci, indicative of replication errors that escaped DNA polymerase proofreading that are being recognized/repaired by MMR. The dependency on MMR function can be rationalized as follows: first, the underrepresented dNTP favors base substitutions and deletion events, and second, the increased concentrations of the other three dNTPs promote mismatch extension independently of the sequence context. In other words, regardless of which base comes after the replication error, DNA polymerases will incorporate, as next, one of the three abundant nucleotides, which will favor mismatch extension over DNA polymerase proofreading and consequently will depend on MMR for repair (Figure 4E).

Among the chromosomally-integrated *rnr1* mutations we identified mutants including *rnr1-K243E* and *rnr1-I262V,N291D* with a '*3 out of 4*' imbalance and extremely elevated dGTP levels, that caused severe mutator phenotypes even in the WT background. These results revealed that this type of imbalance has the strongest mutagenic potential and suggest that increased dGTP concentrations, in the context of a '*3 out of 4*' type of imbalance, correlate with increased mutator phenotypes (Figure 4E). These findings are in agreement with previous work done in *E. coli* (53) that identified a group of particularly mutagenic *nrdA* ribonucleotide reductase mutants with dNTP imbalances characterized by high dGTP and low dATP concentrations associated to reduced cell viability most likely due to the severe accumulation of mutations ('error catastrophe'). Similar to the *rnr1-I262V,N291D* mutant that presented a '*3 out of 4 + extra-high dGTP*' dNTP imbalance, *nrdA-G295S* and *nrdA-A301V* mutants showed a large proportion of A:T to G:C transitions and severe mutation rates in one forward inactivation assay, even in the presence of a functional MMR system. Therefore, this type of dNTP imbalance is particularly mutagenic in *E. coli* as well as in *S. cerevisiae* and potentially also in other organisms.

How may increased dGTP levels in the context of a '*3 out of 4*' imbalance compromise DNA replication fidelity? We envision at least three, not mutually exclusive, potential scenarios:

1. Increased dGTP levels may contribute to the mutagenic dNTP imbalance that may overload the MMR system. This hypothesis is supported by our findings as well as by the previously mentioned study (53) that showed that *nrdA-G295S* and *nrdA-A301V* mutants expressed in either an MMR-proficient or an MMR-deficient background resulted - independently of the MMR status- in increased mutation rates. Moreover, the extreme mutation rates of these *nrdA* mutants were partially suppressed by either overexpression of MutL (one potentially limiting MMR component during the repair reaction) or by expression of an antimutator DNA polymerase mutant (*dnaE925*) that results in an increased DNA replication fidelity (53).
2. Given that dGTP concentrations are the lowest among all four dNTPs, low dGTP concentrations may act as an intrinsic brake, slowing down DNA replication and therefore favoring DNA polymerase proofreading over polymerization. Thus, increased dGTP concentrations may increase the polymerization rate at the expense of replication fidelity.
3. Increased dGTP levels may inhibit DNA polymerase proofreading activity. Previous studies *in vitro* have shown that supplementation of DNA synthesis reactions with dGMP, inhibits polymerase proofreading activity by binding to the exonuclease active site (product inhibition) (54,55). Thus, increased dGTP concentrations may lead to higher dGMP concentrations and reduced proofreading activity. This reduced proofreading activity in combination with a '*3 out of 4*' dNTP imbalance may explain the severe mutator phenotype.

Interestingly, supporting the idea that dGTP levels may play a central role for genome stability, previous work (56,57) reported a positive correlation between intracellular dGTP levels and both telomere length and telomerase processivity *in vivo*. Therefore, it seems that cells have evolved a way to take advantage of the least abundant dNTP (dGTP) to control key processes associated with genome maintenance.

SUPPLEMENTARY DATA

Supplementary Data are available at NAR Online.

ACKNOWLEDGEMENTS

We thank Jessica Williams for thoughtful comments of this manuscript. Thanks to Richard D. Kolodner for strains and reagents and to Annette Kopp-Schneider for advice on statistical analysis. Thanks to Stefan Richter for support on computational modeling of *rnr1* mutations. We are grateful to Sofie Knoll and Frank Exner for technical assistance.

FUNDING

German Cancer Research Center (DKFZ); Marie Curie integration grant 'iMMR' (to H.H.); Swedish Cancer Society; Knut and Alice Wallenberg Foundation and the Swedish Research Council (to A.C.). Funding for open access charge: Deutsches Krebsforschungszentrum.
Conflict of interest statement. None declared.

REFERENCES

1. Kunkel,T.A. and Erie,D.A. (2015) Eukaryotic mismatch repair in relation to DNA replication. *Annu. Rev. Genet.*, **49**, 291–313.
2. Kolodner,R.D. (2016) A personal historical view of DNA mismatch repair with an emphasis on eukaryotic DNA mismatch repair. *DNA Repair (Amst.)*, **38**, 3–13.
3. Reyes,G.X., Schmidt,T.T., Kolodner,R.D. and Hombauer,H. (2015) New insights into the mechanism of DNA mismatch repair. *Chromosoma*, **124**, 443–462.
4. Mathews,C.K. (2006) DNA precursor metabolism and genomic stability. *FASEB J.*, **20**, 1300–1314.
5. Pai,C.C. and Kearsey,S.E. (2017) A critical balance: dNTPs and the maintenance of genome stability. *Genes (Basel)*, **8**, 57–70.
6. Nordlund,P. and Reichard,P. (2006) Ribonucleotide reductases. *Annu. Rev. Biochem.*, **75**, 681–706.
7. Brown,N.C. and Reichard,P. (1969) Role of effector binding in allosteric control of ribonucleoside diphosphate reductase. *J. Mol. Biol.*, **46**, 39–55.
8. Stubbe,J. (2000) Ribonucleotide reductases: the link between an RNA and a DNA world? *Curr. Opin. Struct. Biol.*, **10**, 731–736.
9. Guarino,E., Salguero,I. and Kearsey,S.E. (2014) Cellular regulation of ribonucleotide reductase in eukaryotes. *Semin. Cell Dev. Biol.*, **30**, 97–103.
10. Ahmad,M.F. and Dealwis,C.G. (2013) The structural basis for the allosteric regulation of ribonucleotide reductase. *Prog. Mol. Biol. Transl. Sci.*, **117**, 389–410.
11. Kumar,D., Viberg,J., Nilsson,A.K. and Chabes,A. (2010) Highly mutagenic and severely imbalanced dNTP pools can escape detection by the S-phase checkpoint. *Nucleic Acids Res.*, **38**, 3975–3983.
12. Sanchez,A., Sharma,S., Rozenzhak,S., Roguev,A., Krogan,N.J., Chabes,A. and Russell,P. (2012) Replication fork collapse and genome instability in a deoxycytidylate deaminase mutant. *Mol. Cell. Biol.*, **32**, 4445–4454.
13. Ahluwalia,D., Bienstock,R.J. and Schaaper,R.M. (2012) Novel mutator mutants of E. coli nrdAB ribonucleotide reductase: insight into allosteric regulation and control of mutation rates. *DNA Repair (Amst.)*, **11**, 480–487.
14. Goellner,E.M., Putnam,C.D. and Kolodner,R.D. (2015) Exonuclease 1-dependent and independent mismatch repair. *DNA Repair (Amst.)*, **32**, 24–32.
15. Keijzers,G., Liu,D. and Rasmussen,L.J. (2016) Exonuclease 1 and its versatile roles in DNA repair. *Crit. Rev. Biochem. Mol. Biol.*, **51**, 440–451.
16. Amin,N.S., Nguyen,M.N., Oh,S. and Kolodner,R.D. (2001) exo1-Dependent mutator mutations: model system for studying functional interactions in mismatch repair. *Mol. Cell. Biol.*, **21**, 5142–5155.
17. Schmidt,T.T., Reyes,G., Gries,K., Ceylan,C.U., Sharma,S., Meurer,M., Knop,M., Chabes,A. and Hombauer,H. (2017) Alterations in cellular metabolism triggered by URA7 or GLN3 inactivation cause imbalanced dNTP pools and increased mutagenesis. *Proc. Natl. Acad. Sci. U.S.A.*, **114**, E4442–E4451.
18. Goellner,E.M., Smith,C.E., Campbell,C.S., Hombauer,H., Desai,A., Putnam,C.D. and Kolodner,R.D. (2014) PCNA and Msh2-Msh6 activate an Mlh1-Pms1 endonuclease pathway required for Exo1-independent mismatch repair. *Mol. Cell*, **55**, 291–304.
19. Hombauer,H., Campbell,C.S., Smith,C.E., Desai,A. and Kolodner,R.D. (2011) Visualization of eukaryotic DNA mismatch repair reveals distinct recognition and repair intermediates. *Cell*, **147**, 1040–1053.
20. Janke,C., Magiera,M.M., Rathfelder,N., Taxis,C., Reber,S., Maekawa,H., Moreno-Borchart,A., Doenges,G., Schwob,E., Schiebel,E. *et al.* (2004) A versatile toolbox for PCR-based tagging of yeast genes: new fluorescent proteins, more markers and promoter substitution cassettes. *Yeast*, **21**, 947–962.
21. Sikorski,R.S. and Hieter,P. (1989) A system of shuttle vectors and yeast host strains designed for efficient manipulation of DNA in Saccharomyces cerevisiae. *Genetics*, **122**, 19–27.
22. Muhlrad,D., Hunter,R. and Parker,R. (1992) A rapid method for localized mutagenesis of yeast genes. *Yeast*, **8**, 79–82.
23. Boeke,J.D., LaCroute,F. and Fink,G.R. (1984) A positive selection for mutants lacking orotidine-5′-phosphate decarboxylase activity in yeast: 5-fluoro-orotic acid resistance. *Mol. Gen. Genet.: MGG*, **197**, 345–346.
24. Marsischky,G.T., Filosi,N., Kane,M.F. and Kolodner,R. (1996) Redundancy of Saccharomyces cerevisiae MSH3 and MSH6 in MSH2-dependent mismatch repair. *Genes Dev.*, **10**, 407–420.
25. Rentoft,M., Lindell,K., Tran,P., Chabes,A.L., Buckland,R.J., Watt,D.L., Marjavaara,L., Nilsson,A.K., Melin,B., Trygg,J. *et al.* (2016) Heterozygous colon cancer-associated mutations of SAMHD1 have functional significance. *Proc. Natl. Acad. Sci. U.S.A.*, **113**, 4723–4728.
26. Hombauer,H., Srivatsan,A., Putnam,C.D. and Kolodner,R.D. (2011) Mismatch repair, but not heteroduplex rejection, is temporally coupled to DNA replication. *Science*, **334**, 1713–1716.
27. Eriksson,M., Uhlin,U., Ramaswamy,S., Ekberg,M., Regnstrom,K., Sjoberg,B.M. and Eklund,H. (1997) Binding of allosteric effectors to ribonucleotide reductase protein R1: reduction of active-site cysteines promotes substrate binding. *Structure*, **5**, 1077–1092.
28. Xu,H., Faber,C., Uchiki,T., Fairman,J.W., Racca,J. and Dealwis,C. (2006) Structures of eukaryotic ribonucleotide reductase I provide insights into dNTP regulation. *Proc. Natl. Acad. Sci. U.S.A.*, **103**, 4022–4027.
29. Morrison,A., Johnson,A.L., Johnston,L.H. and Sugino,A. (1993) Pathway correcting DNA replication errors in Saccharomyces cerevisiae. *EMBO J.*, **12**, 1467–1473.
30. Herr,A.J., Kennedy,S.R., Knowels,G.M., Schultz,E.M. and Preston,B.D. (2014) DNA replication error-induced extinction of diploid yeast. *Genetics*, **196**, 677–691.
31. Morrison,A., Bell,J.B., Kunkel,T.A. and Sugino,A. (1991) Eukaryotic DNA polymerase amino acid sequence required for 3′—5′ exonuclease activity. *Proc. Natl. Acad. Sci. U.S.A.*, **88**, 9473–9477.
32. Reenan,R.A. and Kolodner,R.D. (1992) Characterization of insertion mutations in the Saccharomyces cerevisiae MSH1 and MSH2 genes: evidence for separate mitochondrial and nuclear functions. *Genetics*, **132**, 975–985.
33. Zhou,Z. and Elledge,S.J. (1993) DUN1 encodes a protein kinase that controls the DNA damage response in yeast. *Cell*, **75**, 1119–1127.
34. Chabes,A., Georgieva,B., Domkin,V., Zhao,X., Rothstein,R. and Thelander,L. (2003) Survival of DNA damage in yeast directly

depends on increased dNTP levels allowed by relaxed feedback inhibition of ribonucleotide reductase. *Cell*, **112**, 391–401.
35. Tsaponina,O., Barsoum,E., Astrom,S.U. and Chabes,A. (2011) Ixr1 is required for the expression of the ribonucleotide reductase Rnr1 and maintenance of dNTP pools. *PLos Genet.*, **7**, e1002061.
36. Hamel,E., Lustbader,J. and Lin,C.M. (1984) Deoxyguanosine nucleotide analogues: potent stimulators of microtubule nucleation with reduced affinity for the exchangeable nucleotide site of tubulin. *Biochemistry*, **23**, 5314–5325.
37. Caras,I.W. and Martin,D.W. Jr (1988) Molecular cloning of the cDNA for a mutant mouse ribonucleotide reductase M1 that produces a dominant mutator phenotype in mammalian cells. *Mol. Cell. Biol.*, **8**, 2698–2704.
38. Ullman,B., Clift,S.M., Gudas,L.J., Levinson,B.B., Wormsted,M.A. and Martin,D.W. Jr (1980) Alterations in deoxyribonucleotide metabolism in cultured cells with ribonucleotide reductase activities refractory to feedback inhibition by 2′-deoxyadenosine triphosphate. *J. Biol. Chem.*, **255**, 8308–8314.
39. Fairman,J.W., Wijerathna,S.R., Ahmad,M.F., Xu,H., Nakano,R., Jha,S., Prendergast,J., Welin,R.M., Flodin,S., Roos,A. *et al.* (2011) Structural basis for allosteric regulation of human ribonucleotide reductase by nucleotide-induced oligomerization. *Nat. Struct. Mol. Biol.*, **18**, 316–322.
40. Schmidt,T.T. and Hombauer,H. (2016) Visualization of mismatch repair complexes using fluorescence microscopy. *DNA Repair (Amst.)*, **38**, 58–67.
41. Buckland,R.J., Watt,D.L., Chittoor,B., Nilsson,A.K., Kunkel,T.A. and Chabes,A. (2014) Increased and imbalanced dNTP pools symmetrically promote both leading and lagging strand replication infidelity. *PLos Genet.*, **10**, e1004846.
42. Lang,G.I. and Murray,A.W. (2008) Estimating the per-base-pair mutation rate in the yeast Saccharomyces cerevisiae. *Genetics*, **178**, 67–82.
43. Kunkel,T.A. (1992) DNA replication fidelity. *J. Biol. Chem.*, **267**, 18251–18254.
44. Fersht,A.R. (1979) Fidelity of replication of phage phi X174 DNA by DNA polymerase III holoenzyme: spontaneous mutation by misincorporation. *Proc. Natl. Acad. Sci. U.S.A.*, **76**, 4946–4950.
45. Marsischky,G.T. and Kolodner,R.D. (1999) Biochemical characterization of the interaction between the Saccharomyces cerevisiae MSH2-MSH6 complex and mispaired bases in DNA. *J. Biol. Chem.*, **274**, 26668–26682.
46. Jones,M., Wagner,R. and Radman,M. (1987) Repair of a mismatch is influenced by the base composition of the surrounding nucleotide sequence. *Genetics*, **115**, 605–610.
47. Wang,H., Lawrence,C.W., Li,G.M. and Hays,J.B. (1999) Specific binding of human MSH2.MSH6 mismatch-repair protein heterodimers to DNA incorporating thymine- or uracil-containing UV light photoproducts opposite mismatched bases. *J. Biol. Chem.*, **274**, 16894–16900.
48. Mathews,C.K. (2015) Deoxyribonucleotide metabolism, mutagenesis and cancer. *Nat. Rev. Cancer*, **15**, 528–539.
49. Kong,Z., Jia,S., Chabes,A.L., Appelblad,P., Lundmark,R., Moritz,T. and Chabes,A. (2018) Simultaneous determination of ribonucleoside and deoxyribonucleoside triphosphates in biological samples by hydrophilic interaction liquid chromatography coupled with tandem mass spectrometry. *Nucleic Acids Res.*, **46**, e66.
50. Ahmad,M.F., Kaushal,P.S., Wan,Q., Wijerathna,S.R., An,X., Huang,M. and Dealwis,C.G. (2012) Role of arginine 293 and glutamine 288 in communication between catalytic and allosteric sites in yeast ribonucleotide reductase. *J. Mol. Biol.*, **419**, 315–329.
51. Reichard,P. (1988) Interactions between deoxyribonucleotide and DNA synthesis. *Annu. Rev. Biochem.*, **57**, 349–374.
52. Uppsten,M., Farnegardh,M., Jordan,A., Eliasson,R., Eklund,H. and Uhlin,U. (2003) Structure of the large subunit of class Ib ribonucleotide reductase from Salmonella typhimurium and its complexes with allosteric effectors. *J. Mol. Biol.*, **330**, 87–97.
53. Ahluwalia,D. and Schaaper,R.M. (2013) Hypermutability and error catastrophe due to defects in ribonucleotide reductase. *Proc. Natl. Acad. Sci. U.S.A.*, **110**, 18596–18601.
54. Fersht,A.R. and Knill-Jones,J.W. (1983) Contribution of 3′ leads to 5′ exonuclease activity of DNA polymerase III holoenzyme from Escherichia coli to specificity. *J. Mol. Biol.*, **165**, 669–682.
55. Que,B.G., Downey,K.M. and So,A.G. (1978) Mechanisms of selective inhibition of 3′ to 5′ exonuclease activity of Escherichia coli DNA polymerase I by nucleoside 5′-monophosphates. *Biochemistry*, **17**, 1603–1606.
56. Gupta,A., Sharma,S., Reichenbach,P., Marjavaara,L., Nilsson,A.K., Lingner,J., Chabes,A., Rothstein,R. and Chang,M. (2013) Telomere length homeostasis responds to changes in intracellular dNTP pools. *Genetics*, **193**, 1095–1105.
57. Maicher,A., Gazy,I., Sharma,S., Marjavaara,L., Grinberg,G., Shemesh,K., Chabes,A. and Kupiec,M. (2017) Rnr1, but not Rnr3, facilitates the sustained telomerase-dependent elongation of telomeres. *PLos Genet.*, **13**, e1007082.